land

MDPI

Article

Spatiotemporal Analysis of the Coupling Relationship Between Urban Infrastructure and Land Utilization in a Shrinking City: A Case Study of Hegang, Northeast China

Siyi Huang [1,*], Yuefeng Lyu [2], Haokun Shi [1] and Cifang Wu [1,*]

[1] Department of Land Resources Management, School of Public Affairs, Zhejiang University, Hangzhou 310058, China; 11622039@zju.edu.cn
[2] School of Public Administration, Zhejiang University of Finance and Economics, Hangzhou 310018, China; lyuyuefeng@zufe.edu.cn
* Correspondence: huangsiyi@zju.edu.cn (S.H.); wucifang@zju.edu.cn (C.W.)

Abstract: Globally, urbanization is accelerating, with China witnessing a significant 40% rise in urbanization rate over the past 4 decades. However, the dynamic changes in the spatial coupling between infrastructure and utilization intensity during the early, middle, and late stages of urbanization are not clear. The trajectory of development and coupling within the urbanization process is crucial for understanding issues such as urban over-saturation and urban shrinkage. Using Hegang in Northeastern China as an example, we utilized high-resolution remote sensing data, examined the construction intensity of urban land use, analyzed the degree of coupling with utilization efficiency, and clarified the dynamic evolution of the binary relationship system between development and coupling. Results show that Hegang's construction intensity has seen a continuous rise from 1992 to 2000, with a 200.06% increase over 28 years, while its coupling with utilization efficiency has experienced a significant drop in the 21st century, suggesting a persistent decline in the utilization of buildings and a notable urban shrinkage phenomenon. Considering development status and coupling degree, we delineate a characteristic urbanization state curve for Hegang, reflecting its progression through stages of "Underdeveloped, Highly coupled," to "Underdeveloped, Weakly coupled", and finally to "Highly developed, Weakly coupled", offering insights into its urban development path. This research not only establishes a foundational data groundwork for future land-use planning in Hegang but also presents a replicable template for urbanization path analysis in other cities, contributing to a broader understanding of urban development dynamics.

Keywords: built-up land; spatial coupling; construction intensity; nighttime light data; Hegang

Citation: Huang, S.; Lyu, Y.; Shi, H.; Wu, C. Spatiotemporal Analysis of the Coupling Relationship Between Urban Infrastructure and Land Utilization in a Shrinking City: A Case Study of Hegang, Northeast China. *Land* **2024**, *13*, 1904. https://doi.org/10.3390/land13111904

Academic Editor: Jūratė Sužiedelytė-Visockienė

Received: 10 October 2024
Revised: 7 November 2024
Accepted: 11 November 2024
Published: 13 November 2024

1. Introduction

Urbanization is one of the most significant human activities, representing a complex process where rural populations migrate to urban areas and land cover transitions from natural to human-dominated landscapes [1], marking a lifestyle change from agricultural to modern urban living [2–4]. Since the year 2000, an estimated 1.57 billion individuals have transitioned from rural to urban lifestyles, comprising 20.2% of Earth's populace by the year 2020. This demographic shift has led to a 56.4% escalation in urban dwellers throughout the 21st century. Concurrently, there has been a 150% expansion in the world's impervious surface expanse, reaching 108,710 square kilometers. However, the rate of land urbanization does not always align with the rate of population urbanization [1], with urban land expansion either outpacing or lagging behind population growth [5,6]. Additionally, the physical infrastructure of a city, as indicated by its building volume, does not always align with the vitality of its socio-economic status. A low ratio of these two variables indicates an overburdened urban system, which can lead to environmental degradation, food security issues, and climate change challenges [7–9]. Conversely, a large

ratio suggests urban shrinkage, which involves socio-economic issues like population loss [10], economic stagnation [11], and social depression [11] due to factors such as deindustrialization, aging, and suburbanization [12]. Therefore, assessing the spatial coupling between physical construction space and socio-economic vitality over the past decades of urbanization, understanding the relationship between development and coupling, and deploying appropriate mitigation strategies for the increasingly severe urban shrinkage in recent years are essential.

Since the 1980s, China has undergone reform and opening up, compressing into a few decades what normally would take several times longer for urbanization. However, China appears to have experienced excessive urban land expansion [13]. Since 2000, the urban population has increased by 3.8 million (76%), while the urban built-up land area has increased by nearly 300% [1]. Meanwhile, cities in China's northeastern region, with Hegang being the most severe, have experienced significant population outflow, economic decline, and industrial stagnation in the last decade, leading to the emergence of ghost cities and an increasing risk of urban shrinkage. Thus, it represents a typical area worthy of studying the coupling of physical space with socio-economic elements at various stages of urbanization. According to existing research, many scholars typically employ panel data to calculate urban land-use efficiency within the boundaries of an administrative division by integrating various input–output indicators. Common input indicators encompass the area of built-up land [14], fixed asset investment, labor intensity, and energy consumption [15,16]. The output indicators usually include newly added construction land, urban population [17], Gross Domestic Product (GDP), government revenue, and environmental pollution [18]. The models and methods frequently applied include Data Envelopment Analysis (DEA) [16], the Slacks-Based Measure (SBM) model [15], and Stochastic Frontier Analysis (SFA) [18]. However, panel data are characterized by temporal lag and are constrained by administrative boundaries, which limit the richness of information over time and across geographic areas. These limitations make it difficult to capture long-term annual change information and also complicate the identification of specific spatial details at a fine-grained or building-stock level.

Remote sensing data, known for their high spatial and temporal resolution, have become a prevalent tool in urban land use studies, effectively compensating for the shortcomings of panel data. A multitude of land cover products contribute significantly to the comprehensive analysis of urban growth and the transformation of land use and land cover (LULC) [19,20]. Building height data enhance the examination of urban morphology from a vertical perspective, serving as a crucial dimension for assessing the expansion of urban construction volume [21,22]. The year when impervious surfaces were converted provides this study with a timeline of building construction, which aids in the analysis of temporal changes [23]. Moreover, nighttime light data consistently show a robust positive association with population growth and economic vitality [24] and exhibit a strong link to various urban dynamics, including urban form and growth patterns [25], energy usage [26], and carbon emission levels. Gridded Gross Domestic Product (GDP) data can represent the economic activities within each grid cell. These data offer high-resolution, fine-scale insights into urbanization processes over time, surpassing the spatial and temporal precision achievable with traditional panel data analysis. Furthermore, they provide a perspective on long-term coupling dynamics, which is distinct from the single time-point focus of previous studies. Therefore, this study utilizes long-term, high-resolution remote sensing data to focus on the urbanization process in Hegang city from 1992 to 2020, a city that is facing one of the most severe cases of urban shrinkage in the nation. By clarifying the coupling degree between the intensity of infrastructure construction and the city's socioeconomic vitality within each 1km grid cell, this study employs GDP as an indicator of economic output and qualitatively categorizes each grid within a binary framework of development and coupling. This approach delineates a representative urbanization state curve for Hegang, providing insights into its urban development trajectory. Thereafter, we offer suggestions according to the spatial heterogeneity of construction intensity and coupling degree. The

research provides technological guidance for evaluating coupling by fusing multi-source spatial data and lays a foundational data groundwork for future land-use planning in Hegang, offering a replicable template for urbanization path analysis in other cities.

2. Materials and Methods

2.1. Study Area and Data

2.1.1. Study Area

The research was conducted in Hegang, which is located in the northeastern part of Heilongjiang Province, China (Figure 1). The city has six districts and two counties, covering a total area of 14,684 square kilometers. Situated within the "Northeast Sanjiang Plain" formed by the Heilong River, the Songhua River, and the Lesser Khingan Mountains, Hegang borders Russia to the north across the Heilong River. Hegang's economy has historically relied on coal mining and processing, with abundant high-quality coal reserves establishing it as a significant coal production base in China. Historically, the city has been a central energy industrial hub in northeastern Heilongjiang Province. However, the decline of the coal industry has led to significant economic challenges, including population outflow and an urgent need for economic transformation. According to the 2020 census data, the population of Hegang City decreased from 1,058,665 in 2010 to 891,271, a reduction of 167,394 people, which is a 15.81% decrease. Hegang is facing one of the most severe population losses and urban shrinkages in China. How has the coupling of construction intensity and utilization efficiency changed over the last three decades? How has the binary relationship system of development and coupling in Hegang evolved dynamically from 1992 to 2020?

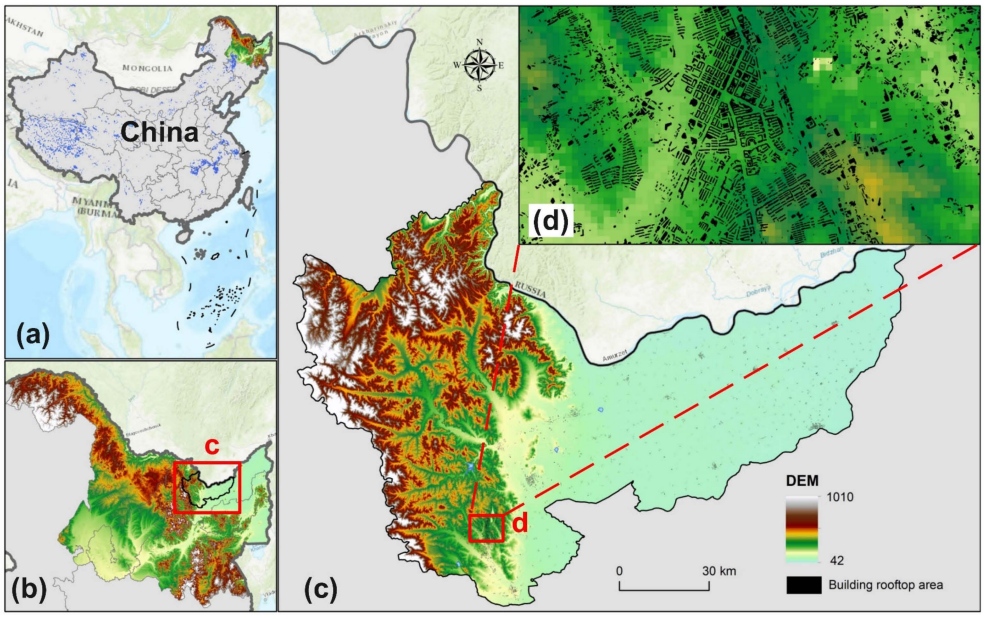

Figure 1. Location of the study area. (**a**) The entire territory of China, (**b**) Heilongjiang Province, (**c**) Hegang City, (**d**) A schematic diagram of rooftops in the center of Hegang City.

In view of the above, this study takes Hegang as an example and tries to analyze the spatio-temporal coupling relationship between its land-use intensity and efficiency, with the hope of providing a reference basis for the construction and development of shrinking cities in China.

2.1.2. Data

The China Building Rooftop Area (CBRA) dataset [27] encompasses a multi-annual collection of rooftop area data with a resolution of 2.5 m, derived from Sentinel-2 satellite imagery spanning from 2016 to 2021. This CBRA dataset is the first to provide full coverage

and multi-annual Building Rooftop Area (BRA) data across China. The high resolution of the data allows for a more precise depiction of the density of planar buildings. Furthermore, this study utilizes the GAIA dataset, produced by Gong et al. [23], to attribute construction years to the CBRA, thereby extracting high-precision building horizontal extents for every two years from 1992 to 2020. The building height data, as reported by Wang et al. [22], complement the three-dimensional form of urban buildings from a vertical perspective. By integrating the horizontal CBRA data, the vertical building height data, and the construction year information from GAIA, a comprehensive three-dimensional dataset of urban buildings constructed year by year is delineated.

The Nighttime Light data (NTL), spanning from 1992 to 2021, is sourced from the unified Global Night Time Lights dataset as reported by Li et al. [28]. The DMSP-OLS and NOAA-VIIRS have been capturing light data from the night sky since 1992 and 2012, respectively. However, due to variations in the spatial detail and sensing technology used by these two sources, a calibration process is essential to ensure data compatibility. The resulting dataset offers a seamless, calibrated sequence of nighttime illumination with a resolution of ~1 km. To mitigate the impact of scattered pixels of nighttime illumination in suburban areas, the study area is further refined. By identifying natural urban boundaries produced by Li et al. [29], a spatially contiguous urban space is selected, thereby avoiding interference from scattered impervious surface pixels in agricultural and ecological spaces.

To characterize the level of urban economic development, we utilized GDP raster data with a spatial resolution of 1 km and a temporal span from 1992 to 2019 [30]. Additionally, we employed the 1 km GDP raster data for China created by Yang et al. as the data source for the final year of our study. Terrain data are collected from SRTMDEM 90M resolution raw elevation data, which is part of the Shuttle Radar Topography Mission (SRTM), an international project executed by NASA and the National Geospatial-Intelligence Agency (NGA). The administrative boundary data are collected from http://www.resdc.cn/ (accessed on 10 July 2024). The specific data types and sources are shown in Table 1.

Table 1. Data and sources.

Data	Type	Resolution	Unit	Source
China Building Rooftop Area (CBRA)	Raster	2.5 m	0/1	Liu et al. [27]
GAIA	Raster	30 m	Year	Gong et al. [23]
Building height data	Raster	1 km	m	Wang et al. [22]
Nighttime Light Data (NTL)	Raster	1 km	DN value	Harmonized Global Night Time Lights (1992–2021)—awesome-gee-community-catalog [28]
Urban boundaries	Vector	/	/	Li et al. [29]
GDP	Raster	1 km	Yuan	Chen et al. [30] & https://doi.org/10.6084/m9.figshare.21485682.v1 (accessed on 10 July 2024)
DEM	Raster	90 m	m	http://www.gscloud.cn/ (accessed on 10 July 2024)
Administrative boundary	Vector	/	/	http://www.resdc.cn/ (accessed on 10 July 2024)

2.2. Methodology Framework

This study is structured into four steps, conducting a long-term sequence analysis of land-use changes in Hegang from 1992 to 2020 across four dimensions: construction intensity (measured by Built-up Volume, BUV), its coupling with actual utilization intensity (measured by Lighted Building Index, LBI), the evolution of the binary relationship between

coupling and development over the past three decades, and the spatial autocorrelation of both BUV and LBI annually. The detailed technical framework is shown in Figure 2.

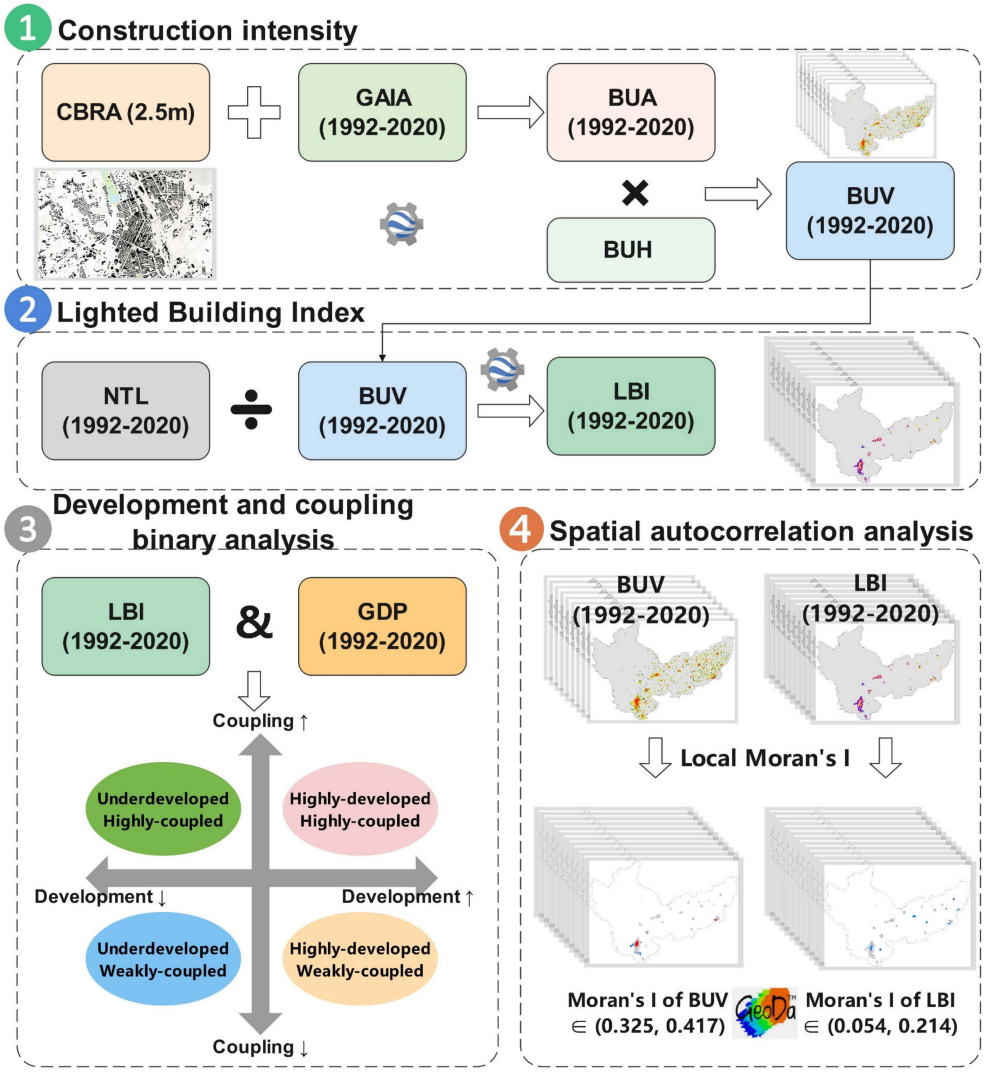

Figure 2. Technical framework.

2.2.1. Construction Intensity of Urban Built-Up Land

We used the 2021 CBRA to represent the existing rooftop areas as of that year. Since GAIA indicates the year of construction for buildings (ranging from 1985 to 2022 on an annual basis), overlaying the CBRA with GAIA allows us to assign the construction date information from GAIA to the corresponding locations in the CBRA. This enables us to obtain rooftop area data for any desired analysis year, resulting in Built-up Area (BUA) for every two-year interval from 1992 to 2020. The intensity of urban construction land use is represented by Built-up Volume (BUV) [31,32]. BUV is calculated as the product of the Built-up Area (BUA) on the horizontal plane and the Built-up Height (BUH) on the vertical plane within a 1 km by 1 km grid. The formula is as follows:

$$BUV = BUA \times BUH, \quad (1)$$

where BUA represents the total area of building rooftops within a 1 km grid for each year, measured in square meters (m^2); BUH represents the average height of buildings within the 1 km grid, measured in meters (m); BUV represents the total volume of buildings within a 1 km grid for each year, measured in cubic meters (m^3). BRA refers to the Constructed Building Rooftop Area with a 2.5 m resolution data set within the 1 km grid for each

year. TA is the total area of the 1 km grid. Calculations are performed for every even year between 1992 and 2020, encompassing a total of 15 years of data.

2.2.2. Lighted Building Index

We utilize Nighttime Light data (NTL) to characterize the actual utilization of urban construction land within each 1km grid cell. The Lighted Building Index (LBI) is a metric we have developed in this study to reflect the efficiency of light utilization per unit of construction volume. It is calculated by taking the ratio of Nighttime Lights (NTL) to Built-up Volume (BUV). This study employs LBI to quantify the coupling between construction intensity and actual utilization, attempting to conduct a long-term coupling analysis from 1992 to 2020 (Equation (3)).

$$LBI = \frac{NTL}{BUV}, \tag{2}$$

where LBI represents Lighted Building Index (unit: DN value/m^3); NTL refers to Nighttime Light data, which is typically derived from the fusion of two commonly used remote sensing sources, DMSP-OLS and NPP-VIIRS. BUV represents the total volume of buildings within a 1 km grid for each year, calculated in Section 2.2.1. To mitigate the impact of scattered pixels of nighttime illumination in suburban areas during the calculation of the Landscape Biodiversity Index (LBI), the study area is further refined. By identifying natural urban boundaries, a spatially contiguous urban space is selected, thereby avoiding interference from scattered impervious surface pixels in agricultural and ecological spaces.

2.2.3. Bivariate Quadrant Trajectory Analysis

We conducted an integrated analysis of the binary relationship between the total GDP and the Lighted Building Index (LBI) in Hegang City from 1992 to 2020. The two-dimensional space defined by these two indicators was divided into four quadrants, representing 'Highly developed, Highly coupled', 'Highly developed, Weakly coupled', 'Underdeveloped, Highly coupled', and 'Underdeveloped, Weakly coupled'. By performing pixel-by-pixel time series analysis and spatial time series analysis on the GDP and LBI data for every other year over the 1992–2020 period, spanning 15 phases, we mapped out the developmental trajectories across different years. From these analyses, we summarized the evolution of the relationship between coupling and development.

2.2.4. Spatial Autocorrelation Analysis

Spatial autocorrelation analysis, including Moran's I and Local Moran's I, are utilized to examine the variability in spatial distribution of Built-up Volume (BUV) and the Lighted Building Index (LBI). Moran's I assesses the overall spatial clustering within the data, identifying whether values are concentrated in specific areas or dispersed randomly. Local Moran's I, on the other hand, identifies specific spatial units with high or low values relative to their neighbors, revealing distinct spatial association patterns. The calculation of Moran's I is as follows:

$$I = \frac{n}{\sum_{i=1}^{n}\sum_{j=1}^{n} w_{ij}} \times \frac{\sum_{i=1}^{n}\sum_{j=1}^{n} w_{ij}(x_i - \overline{x})(x_j - \overline{x})}{\sum_{i=1}^{n}(x_i - \overline{x})^2}, \tag{3}$$

where I represents Moran's I, which is calculated based on the number of spatial units n within the study area. The value of the ith spatial unit is represented by x_i, while $\overline{x}$ represents the average value across all units. The matrix of spatial weights is denoted by w_{ij}. The selection of the weight matrix is to serve the purpose of explaining spatial autocorrelation. In this study, we considered the use of the adjacency matrix, which effectively reflects the adjacency relationships between observations in spatial data. Specifically, the adjacency matrix is defined based on the boundary contact between regions. If two regions share a boundary, we set $w_{ij} = 1$; otherwise, $w_{ij} = 0$.

The calculation of Local Moran's I is as follows:

$$I_i = \frac{x_i - \overline{x}}{\left(\frac{\sum_{i=1}^{n}(x_i-\overline{x})^2}{n}\right)} \times \sum_{i=1}^{n}\sum_{j=1}^{n} w_{ij}(x_j - \overline{x}), \quad (4)$$

where the Local Moran's I index for the *i*th spatial unit, denoted as I_i, uses the same parameters as previously defined for the Moran's I calculation.

3. Results

3.1. Spatiotemporal Construction Intensity of Urban Built-Up Land

Integrating the horizontal expansion and vertical height of construction land, the results of Built-up Volume (BUV) are illustrated in Figure 3. The construction intensity in Hegang city has been increasing year by year from 1992 to 2020, characterized by a gradual increase in the number of pixels containing buildings and a year-on-year increase in the construction intensity of existing building pixels. Spatially, the northwest region, dominated by the mountainous area of the Lesser Khingan Range, has rugged terrain and less construction land; the southern main urban area is the region with the highest construction intensity in the city; the eastern region is a grain planting development area, mainly plain, with scattered patches of construction land. Over time, the average BUV in Hegang has risen from 204.5 $\times$ 10^3 m^3 in 1992 to 410.3 $\times$ 10^3 m^3 in 2020, an increase of 200.6% over 28 years. Based on the natural break method, construction land is divided into 10 categories. Taking the BUV distribution in 1992 and 2020 as examples, the top 1 category of BUV values (BUV > 240 $\times$ 10^3 m^3) is mainly concentrated in the central area of Hegang city and the centers of various counties, accounting for 22.2% of the total construction land area in 1992 and 45.5% in 2020; In contrast, the lowest category of BUV values (BUV < 1 $\times$ 10^3 m^3) is mainly sporadically found in rural construction land, accounting for 13.5% of the total construction land area in 1992 and 1.9% in 2020. Construction land with moderate BUV exists in the transitional areas between the aforementioned two, that is, the urban–rural fringe areas on the edge of the city. The construction intensity has surged over the span of 28 years, affecting not only the city center but also the suburban areas and the scattered rural construction sites.

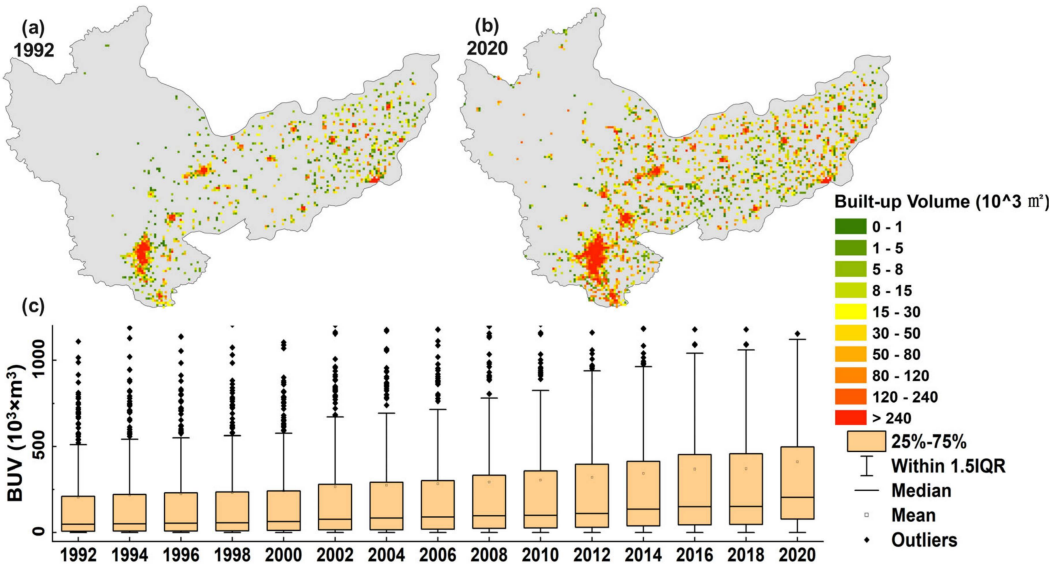

Figure 3. Spatiotemporal distribution of Built-up Volume (BUV) in Hegang city from 1992 to 2020. (**a**,**b**) represent the spatial distribution of BUV for construction land in Hegang for the year 1992 and 2020, respectively; (**c**) BUV statistics of build-up land pixels per year.

3.2. The Coupling Between Construction and Actual Utilization

The Lighted Building Index (LBI) in Hegang city has shown an overall trend of increasing initially and then decreasing (Figure 4), representing a pattern where the coupling

degree between urban construction volume and actual utilization first increased and then decreased. Between 1992 and 1998, both the average and median LBI values in Hegang increased significantly. However, from 2000 to 2020, there was a noticeable decline. By 2020, the mean LBI had dropped to 1.68×10^{-3}, which is only 40.5% of its value in 1992 (4.15×10^{-3}), indicating a severe phenomenon of urban shrinkage in Hegang during the 21st century. By 2020 (Figure 4b), the pixels with the lowest LBI values were concentrated in the central area of Hegang city, suggesting that the city center, which should be the most vibrant, is now the most affected by urban shrinkage. This central decline in the LBI is indicative of a larger trend where the areas that were once economic and social hubs are now experiencing a significant reduction in activity and investment. The concentration of low LBI values in the city center could be a result of various factors such as depopulation, economic downturn, or a shift in economic activities to other regions within or outside the city. Moreover, Figure 4c tracks the changes in the LBI over the 28-year period for the top 10 1 km pixels with the highest LBI values in 1992. The top three pixels experienced a dramatic decrease in LBI after the turn of the century. The combined LBI of the top 10 pixels was 1.35 in 1992, with an average value of 0.13; by 2020, this sum and average had reduced to 0.18 and 0.02, respectively. These figures represent only 13.3% and 15.4% of their values in 1992, indicating a more severe decline than the overall mean LBI value for all pixels in Hegang.

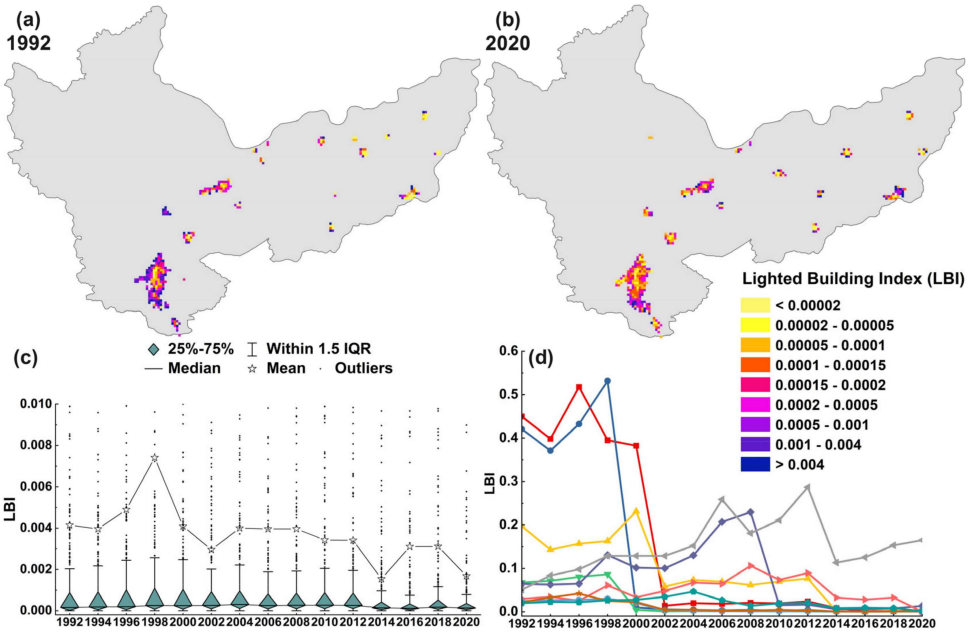

Figure 4. Spatiotemporal distribution of the Lighted Building Index (LBI) in Hegang city from 1992 to 2020. (**a**,**b**) represent the spatial distribution of the LBI for construction land in Hegang for the year 1992 and 2020, respectively; (**c**) LBI statistics of build-up land pixels per year; (**d**) Temporal changes in the LBI from 1992 to 2020 for the top 10 pixels with the highest LBI values in Hegang in 1992.

3.3. The Evolution of the Relationship Between Coupling and Development

The average LBI and the total GDP from 1992 to 2020 can reflect the urban land-use coupling degree and the level of economic development, respectively (Figure 5a). Over the period from 1992 to 2020, the coupling degree generally showed a downward trend, while GDP, despite a decline in 2014, has generally been on an upward trajectory. In terms of spatial correlation, Figure 5b shows that pixels with higher GDP in the city center have a lower LBI, whereas pixels with lower GDP in the urban–rural fringe and suburban areas have a higher LBI. This phenomenon may be attributed to excessive construction in the city center due to overconfidence on the part of local governments and fiscal incentives.

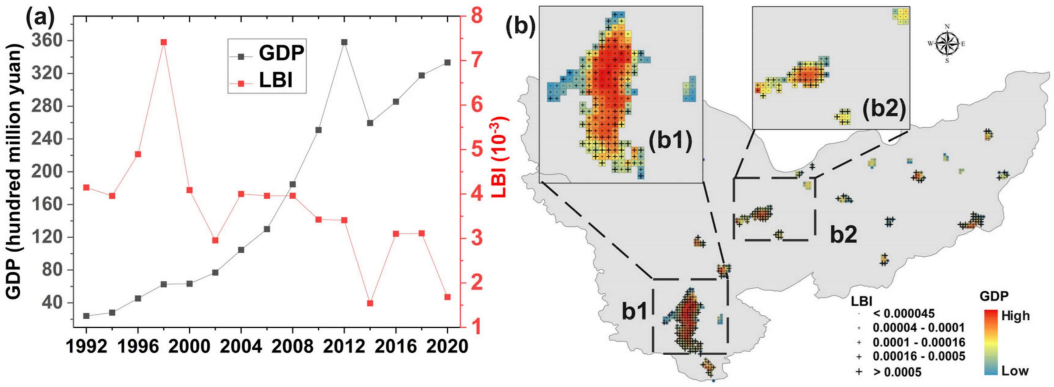

Figure 5. The spatiotemporal differentiation of GDP and LBI in Hegang. (**a**) Time series changes in GDP and LBI from 1992 to 2020; (**b**) The spatial correspondence between GDP and LBI; (**b1**) The center of Hegang City; (**b2**) Sub-center of Hegang City.

We utilized the biennial LBI and GDP of Hegang as the two axes, dividing the space into four quadrants, which represent 'Highly developed, Highly coupled', 'Highly developed, Weakly coupled', 'Underdeveloped, Highly coupled', and 'Underdeveloped, Weakly coupled'. Based on the changes in the two factors for Hegang each year, we can delineate its position within the four quadrants. By connecting these positions over time, we can illustrate the transformation trajectory of Hegang over the past 28 years. Overall, Hegang has experienced three developmental stages from 1992 to 2020: "Underdeveloped, Highly coupled", "Underdeveloped, Weakly coupled", and "Highly developed, Weakly coupled" (Figure 6). Initially, before the 21st century, Hegang was limited by traditional economic constraints, resulting in a low GDP, lower construction intensity, and lower urban building utilization. However, the Lighted Building Index (LBI), an indicator of the utilization per unit of construction volume, was relatively high, suggesting a state of low-level coupling. Thereafter, in the first decade of the 21st century, driven by the broader economic environment in China, Hegang's economy began to improve rapidly. With the incentive of land finance, a large number of new buildings were constructed, but actual utilization did not keep pace with construction intensity, reflected by a decrease in the LBI, indicating a state of low-level decoupling. After 2010, Hegang's economy further improved, with the total GDP exceeding 200 billion yuan. Although GDP declined in 2014, it can be generally recognized that the city entered a high-level stage. However, facing significant population outflow and urban shrinkage, LBI saw a sharp decline, with the 2020 LBI being approximately one-quarter of that in 2010, indicating a state of high-level decoupling. Therefore, in the development process over the past 30 years, Hegang has gone through three stages, with the notable absence of a high-level coupling state.

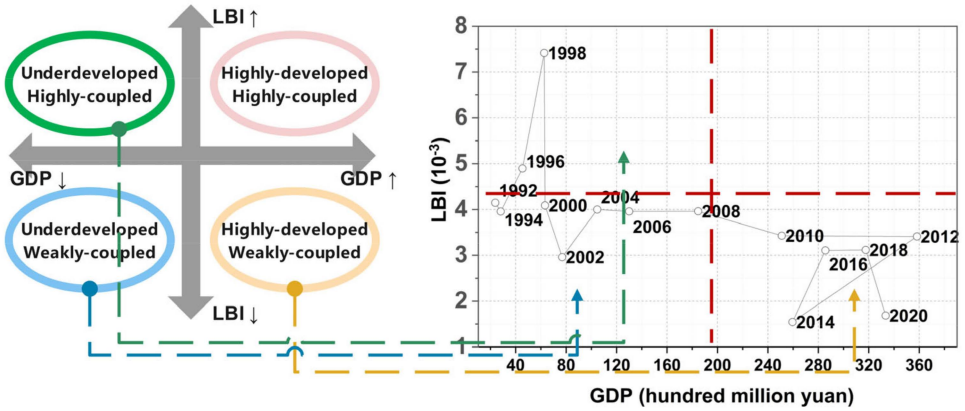

Figure 6. The transformation pathways of Hegang between four coupling−development models from 1992 to 2020.

3.4. Spatial Autocorrelation

Based on Moran's I, BUV and the LBI are positively spatially correlated, respectively, i.e., the higher values of BUV are associated with a greater tendency for pixels to cluster, while the lower LBI values are associated with a greater tendency for pixels to cluster. Specifically, the Moran's I value for BUV from 1992 to 2020 ranges from 0.325 to 0.417, while for the LBI it ranges from 0.054 to 0.214. The results from the Local Moran's I analysis reveal the spatial clustering of Built-up Volume (BUV) and the Lighted Building Index (LBI), highlighting the spatial characteristics of built-up land construction intensity (Figure 7a,c,e,g) and the coupling between building and utilization (Figure 7b,d,f,h). Both BUV and the LBI exhibit spatial agglomeration. The spatial pattern of agglomeration for BUV and the LBI is such that they share the same spatial locations but exhibit opposite values. This implies that pixels which are high-high clusters for BUV are, in contrast, low-low clusters for the LBI. This phenomenon illustrates that areas with high construction intensity, primarily centered around the city center, are paradoxically areas of low coupling, as shown in the low LBI values. This is corroborated by the GDP high-value areas in 2020 (as depicted in Figure 5b), which also coincide with lowLBI-value areas, illustrating a disconnect between the physical space and economic vitality in the city of Hegang from two different perspectives.

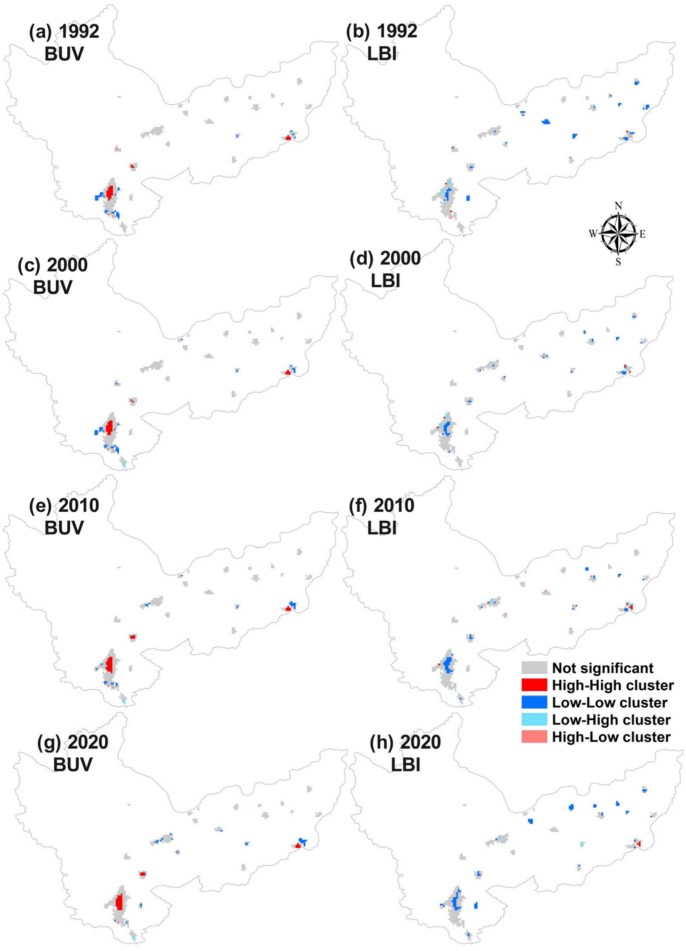

Figure 7. Local Moran's I of BUV and LBI in 1992, 2000, and 2020.

4. Discussion

4.1. Analyzing Longitudinal Urbanization from the Perspective of Spatial Coupling

Relying on long-time, high-resolution remote sensing images, the aim of this study is to analyze the spatial coupling between the physical space of a shrinking city and its actual utilization. While gridded GDP data inevitably introduce errors during their production

and distribution process, making them less accurate in reflecting utilization intensity compared to nighttime light data (NTL), NTL, on the other hand, consistently show a robust positive association with population growth and economic vitality [24] and exhibit a strong link to various urban dynamics, including urban form and growth patterns [25], energy usage [26], and carbon emission levels. We employ a 1 km resolution NTL dataset spanning from 1992 to 2020. This dataset is instrumental in analyzing the actual utilization corresponding to the Built-up Volume (BUV) within 1 km grids. Our methodology incorporates a biennial monitoring frequency, an approach that adeptly captures temporal dynamics without redundancy, thus making it scalable to broader regions. Additionally, we have scaled up 2.5 m resolution rooftop data to align with the 1 km grid scale of our NTL data. This upscaling process is critical as it harmonizes with the NTL dataset and minimizes granular errors, ensuring a more accurate representation of BUV. In the calculation of BUV within the 1 km grids, the precision of horizontal building footprints is paramount, significantly influencing the determination of building volume. Recognizing the absence of Chinese regional building contour data in several globally recognized datasets, such as Microsoft's [33] and Google's dataset [34], we have opted for 2.5 m resolution building rooftop data [27]. These higher-resolution data provide a precise delineation of each building's outline, enhancing the precision of construction intensity calculations. By comparing the LBI and GDP within the identical 1 km grid locations, we qualitatively categorized each grid within a binary framework of development and coupling. Utilizing time series data from 1992 to 2020, we have classified the urbanization states of individual grids and the city as a whole over this period. Our findings reveal that Hegang has traversed an urbanization trajectory characterized by stages of "Underdeveloped, Highly coupled", "Underdeveloped, Weakly coupled", and "Highly developed, Weakly coupled", now confronting an escalated risk of urban contraction. Previous studies typically employ panel data to calculate urban land-use efficiency within the boundaries of an administrative division by integrating various input–output indicators. However, panel data are characterized by temporal lag and are constrained by administrative boundaries, which limit the richness of information over time and across geographic areas. This study addresses these challenges by utilizing multi-source long-term and high-resolution remote sensing data, which not only sets a precedent for urbanization studies but also lays a foundational data groundwork for future land-use planning in Hegang, offering a replicable template for urbanization path analysis in other cities.

4.2. Policy Implications

Over the past 28 years, the construction intensity of Hegang city has continuously increased, yet the actual utilization per unit of building space, as indicated by the Lighted Building Index (LBI), has been decreasing throughout this century. Moreover, the spatial heterogeneity demonstrates that areas with high construction intensity, primarily centered around the city center, are paradoxically areas of low coupling, as shown in the low LBI values. This is corroborated by the GDP high-value areas in 2020, which also coincide with low-LBI-value areas, illustrating a disconnect between the physical space and economic vitality in the city of Hegang from two different perspectives. Temporally, the degree of mismatch between the city's physical space and its economic vitality has been escalating, with Hegang facing some of the most severe urban shrinkage issues observed both nationally and globally. The Moran's I value for BUV and the LBI both increased, demonstrating that spatial heterogeneity within the administrative region of Hegang is becoming more severe. Against this backdrop, the Hegang government's continued reliance on traditional incremental planning is likely to exacerbate the disconnection between people and the land in the future. Looking ahead, the local government of Hegang should shift from the traditional land finance-driven extensive growth model to a more refined and sustainable urban development strategy. Like many other resource-oriented cities such as Karamay [35] and Datong [36], Hegang needs to transition into a more compact city. This includes enhancing the optimization of existing building spaces, improving the intensity and efficiency of

actual use of construction and focusing on elevating the quality of life for residents to create a more livable urban environment. The government must prioritize a balance between urban planning and land use, curb unregulated expansion, and mitigate the disconnection between urban spaces and human-land relationships. Through these measures, Hegang can gradually alleviate the pressures of urban contraction and forge a path of sustainable development that meets the demands of the new era. This study provides insights for the development and construction of second-tier cities, as well as for the allocation of national land use indicators.

5. Conclusions

This study utilizes long-term, high-resolution remote sensing data to focus on the urbanization process in Hegang city from 1992 to 2020. By clarifying the coupling degree between the intensity of infrastructure construction (BUV, which has seen a continuous rise with a 200.06% increase over 28 years) and the city's socioeconomic vitality (NTL), we conducted a quantitative analysis of the Lighted Building Index (LBI) across each 1 km grid cell over the past 28 years. Our findings indicate that the LBI initially increased and subsequently decreased, with a significant drop in the 21st century, suggesting a persistent decline in the utilization of buildings and a notable urban shrinkage phenomenon. Additionally, the study uses GDP as an economic output indicator and qualitatively categorizes each grid within a binary framework of development and coupling. This methodology has allowed us to delineate a characteristic urbanization state curve for Hegang, reflecting its progression through stages of "Underdeveloped, Highly coupled", to "Underdeveloped, Weakly coupled", and finally to "Highly developed, Weakly coupled", offering insights into its urban development path. The spatial autocorrelation results reveal that the local Moran's I for BUV and the LBI share the same spatial locations but exhibit opposite values. That is, pixels identified as high-high clusters for BUV are, conversely, low-low clusters for the LBI, indicating that the central urban construction areas are the most severely affected by hollowing out and the emergence of ghost towns. Accordingly, we provide recommendations tailored to the spatial heterogeneity of construction intensity and coupling degree.

This study, while offering novel insights, has some limitations. For example, the Nighttime Light (NTL) data we relied upon are susceptible to the spatial saturation effect, which can overstate the brightness levels in areas with lower nighttime illumination. Moreover, the NTL values, being based on artificial light emissions, may not accurately reflect the economic activity in industrial zones and commercial districts with minimal nighttime activity, potentially leading to an underestimation of their actual utilization. Moreover, building rooftop data are selected as the focus of this research; however, the study does not differentiate between urban and rural rooftops. Consequently, a notable portion of rural built-up land with low BUV is inadvertently included in the analysis. In future work, we will refine our methodology to mitigate the limitations of NTL data, employing additional datasets and analytical techniques to provide a more accurate and comprehensive assessment of urban spatial dynamics. Moreover, we plan to expand our research framework to include a broader geographical scope, aiming to analyze urban coupling degrees across different cities on a regional and national scale. This will enable a comparative study of urban development trends and spatial coupling evolution over the past three decades, offering valuable data for urban planning and policymaking, steering towards sustainable urban growth. Overall, this research offers technical guidance for evaluating coupling by integrating multi-source spatial data, establishing a foundational data groundwork for future land-use planning in Hegang. It also presents a replicable template for urbanization path analysis in other cities, contributing to a broader understanding of urban development dynamics.

Author Contributions: Conceptualization, S.H. and C.W.; methodology, Y.L.; software, S.H. and Y.L.; validation, S.H., Y.L. and H.S.; formal analysis, S.H.; data curation, H.S.; writing—original draft preparation, S.H.; writing—review and editing, Y.L.; visualization, H.S.; supervision, C.W.; project administration, C.W. All authors have read and agreed to the published version of the manuscript.

Funding: This research was funded by The National Natural Science Foundation of China, Grant No. 42401120 and Zhejiang Provincial Natural Science Foundation of China, Grant No. Q24D010026.

Data Availability Statement: Data will be made available on request.

Conflicts of Interest: The authors declare no conflict of interest.

References

1. Ruan, L.; He, T.; Xiao, W.; Chen, W.; Lu, D.; Liu, S. Measuring the Coupling of Built-up Land Intensity and Use Efficiency: An Example of the Yangtze River Delta Urban Agglomeration. *Sustain. Cities Soc.* **2022**, *87*, 104224. [CrossRef]
2. Buhaug, H.; Urdal, H. An Urbanization Bomb? Population Growth and Social Disorder in Cities. *Glob. Environ. Change* **2013**, *23*, 1–10. [CrossRef]
3. Dadashpoor, H.; Azizi, P.; Moghadasi, M. Land Use Change, Urbanization, and Change in Landscape Pattern in a Metropolitan Area. *Sci. Total Environ.* **2019**, *655*, 707–719. [CrossRef] [PubMed]
4. Hatuka, T.; Zur, H.; Mendoza, J.A. The Urban Digital Lifestyle: An Analytical Framework for Placing Digital Practices in a Spatial Context and for Developing Applicable Policy. *Cities* **2021**, *111*, 102978. [CrossRef]
5. Hennig, E.I.; Schwick, C.; Soukup, T.; Orlitová, E.; Kienast, F.; Jaeger, J.A.G. Multi-Scale Analysis of Urban Sprawl in Europe: Towards a European de-Sprawling Strategy. *Land Use Policy* **2015**, *49*, 483–498. [CrossRef]
6. Seto, K.C.; Fragkias, M.; Güneralp, B.; Reilly, M.K. A Meta-Analysis of Global Urban Land Expansion. *PLoS ONE* **2011**, *6*, e23777. [CrossRef]
7. Bai, X.; McPhearson, T.; Cleugh, H.; Nagendra, H.; Tong, X.; Zhu, T.; Zhu, Y.-G. Linking Urbanization and the Environment: Conceptual and Empirical Advances. *Annu. Rev. Environ. Resour.* **2017**, *42*, 215–240. [CrossRef]
8. Deng, X.; Huang, J.; Rozelle, S.; Zhang, J.; Li, Z. Impact of Urbanization on Cultivated Land Changes in China. *Land Use Policy* **2015**, *45*, 1–7. [CrossRef]
9. Sun, R.; Lü, Y.; Yang, X.; Chen, L. Understanding the Variability of Urban Heat Islands from Local Background Climate and Urbanization. *J. Clean. Prod.* **2019**, *208*, 743–752. [CrossRef]
10. Sutradhar, U.; Spearing, L.; Derrible, S. Depopulation and Associated Challenges for US Cities by 2100. *Nat. Cities* **2024**, *1*, 51–61. [CrossRef]
11. Jiang, Z.; Zhai, W.; Meng, X.; Long, Y. Identifying Shrinking Cities with NPP-VIIRS Nightlight Data in China. *J. Urban Plan. Dev.* **2020**, *146*, 04020034. [CrossRef]
12. Niva, V.; Horton, A.; Virkki, V.; Heino, M.; Kosonen, M.; Kallio, M.; Kinnunen, P.; Abel, G.J.; Muttarak, R.; Taka, M.; et al. World's Human Migration Patterns in 2000–2019 Unveiled by High-Resolution Data. *Nat. Hum. Behav.* **2023**, *7*, 2023–2037. [CrossRef] [PubMed]
13. Li, Y.; Pu, S.; Zhao, Y.; Yao, J.; Qian, K. Refractive-Index-Matched Coupling Generated by Magnetic Fluid around Cladding Removed Multimode Optical Fiber. *Opt. Fiber Technol.* **2020**, *59*, 102326. [CrossRef]
14. Masini, E.; Tomao, A.; Barbati, A.; Corona, P.; Serra, P.; Salvati, L. Urban Growth, Land-Use Efficiency and Local Socioeconomic Context: A Comparative Analysis of 417 Metropolitan Regions in Europe. *Environ. Manag.* **2019**, *63*, 322–337. [CrossRef]
15. Jiang, H. Spatial–Temporal Differences of Industrial Land Use Efficiency and Its Influencing Factors for China's Central Region: Analyzed by SBM Model. *Environ. Technol. Innov.* **2021**, *22*, 101489. [CrossRef]
16. Zhu, X.; Zhang, P.; Wei, Y.; Li, Y.; Zhao, H. Measuring the Efficiency and Driving Factors of Urban Land Use Based on the DEA Method and the PLS-SEM Model—A Case Study of 35 Large and Medium-Sized Cities in China. *Sustain. Cities Soc.* **2019**, *50*, 101646. [CrossRef]
17. Du, Y.; Li, B.; Chen, M. Surges Induced in Building Electrical Systems during a Lightning Strike. *Electr. Power Syst. Res.* **2016**, *139*, 68–74. [CrossRef]
18. Liu, S.; Xiao, W.; Li, L.; Ye, Y.; Song, X. Urban Land Use Efficiency and Improvement Potential in China: A Stochastic Frontier Analysis. *Land Use Policy* **2020**, *99*, 105046. [CrossRef]
19. Kussul, N.; Lavreniuk, M.; Skakun, S.; Shelestov, A. Deep Learning Classification of Land Cover and Crop Types Using Remote Sensing Data. *IEEE Geosci. Remote Sens. Lett.* **2017**, *14*, 778–782. [CrossRef]
20. Xu, M.; Yang, Y.; Deng, Q.-W.; Shen, J.-T.; Liu, W.-F.; Yang, W.-J.; Liu, K.-X. Microarray Profiling and Functional Identification of LncRNA in Mice Intestinal Mucosa Following Intestinal Ischemia/Reperfusion. *J. Surg. Res.* **2021**, *258*, 389–404. [CrossRef]
21. Esch, T.; Zeidler, J.; Palacios-Lopez, D.; Marconcini, M.; Roth, A.; Mönks, M.; Leutner, B.; Brzoska, E.; Metz-Marconcini, A.; Bachofer, F. Towards a Large-Scale 3D Modeling of the Built Environment—Joint Analysis of TanDEM-X, Sentinel-2 and Open Street Map Data. *Remote Sens.* **2020**, *12*, 2391. [CrossRef]
22. Wang, K.; He, T.; Xiao, W.; Yang, R. Projections of Future Spatiotemporal Urban 3D Expansion in China under Shared Socioeconomic Pathways. *Landsc. Urban Plan.* **2024**, *247*, 105043. [CrossRef]
23. Gong, P.; Li, X.; Wang, J.; Bai, Y.; Chen, B.; Hu, T.; Liu, X.; Xu, B.; Yang, J.; Zhang, W.; et al. Annual Maps of Global Artificial Impervious Area (GAIA) between 1985 and 2018. *Remote Sens. Environ.* **2020**, *236*, 111510. [CrossRef]
24. Chen, Z.; Yu, B.; Ta, N.; Shi, K.; Yang, C.; Wang, C.; Zhao, X.; Deng, S.; Wu, J. Delineating Seasonal Relationships Between Suomi NPP-VIIRS Nighttime Light and Human Activity Across Shanghai, China. *IEEE J. Sel. Top. Appl. Earth Obs. Remote Sens.* **2019**, *12*, 4275–4283. [CrossRef]

25. Zhang, Q.; Fang, K.; Chen, J.; Liu, H.; Liu, P. The Role of Sectoral Coverage in Emission Abatement Costs: Evidence from Marginal Cost Savings. *Environ. Res. Lett.* **2022**, *17*, 045002. [CrossRef]
26. Jasiński, T. Modeling Electricity Consumption Using Nighttime Light Images and Artificial Neural Networks. *Energy* **2019**, *179*, 831–842. [CrossRef]
27. Liu, Z.; Tang, H.; Feng, L.; Lyu, S. China Building Rooftop Area: The First Multi-Annual (2016–2021) and High-Resolution (2.5 m) Building Rooftop Area Dataset in China Derived with Super-Resolution Segmentation from Sentinel-2 Imagery. *Earth Syst. Sci. Data* **2023**, *15*, 3547–3572. [CrossRef]
28. Li, X.; Zhou, Y.; Zhao, M.; Zhao, X. Harmonization of DMSP and VIIRS Nighttime Light Data from 1992–2020 at the Global Scale. *Sci. Data* **2020**, *7*, 168. [CrossRef]
29. Li, X.; Gong, P.; Zhou, Y.; Wang, J.; Bai, Y.; Chen, B.; Hu, T.; Xiao, Y.; Xu, B.; Yang, J.; et al. Mapping Global Urban Boundaries from the Global Artificial Impervious Area (GAIA) Data. *Environ. Res. Lett.* **2020**, *15*, 094044. [CrossRef]
30. Chen, J.; Gao, M.; Cheng, S.; Hou, W.; Song, M.; Liu, X.; Liu, Y. Global 1 Km × 1 Km Gridded Revised Real Gross Domestic Product and Electricity Consumption during 1992–2019 Based on Calibrated Nighttime Light Data. *Sci. Data* **2022**, *9*, 202. [CrossRef]
31. Dutta, D.; Rahman, A.; Paul, S.K.; Kundu, A. Estimating Urban Growth in Peri-Urban Areas and Its Interrelationships with Built-up Density Using Earth Observation Datasets. *Ann. Reg. Sci.* **2020**, *65*, 67–82. [CrossRef]
32. Geiß, C.; Leichtle, T.; Wurm, M.; Pelizari, P.A.; Standfuß, I.; Zhu, X.X.; So, E.; Siedentop, S.; Esch, T.; Taubenböck, H. Large-Area Characterization of Urban Morphology—Mapping of Built-Up Height and Density Using TanDEM-X and Sentinel-2 Data. *IEEE J. Sel. Top. Appl. Earth Obs. Remote Sens.* **2019**, *12*, 2912–2927. [CrossRef]
33. GlobalMLBuildingFootprints. Available online: https://github.com/microsoft/GlobalMLBuildingFootprints (accessed on 10 August 2024).
34. Sirko, W.; Kashubin, S.; Ritter, M.; Annkah, A.; Bouchareb, Y.S.E.; Dauphin, Y.; Keysers, D.; Neumann, M.; Cisse, M.; Quinn, J. Continental-Scale Building Detection from High Resolution Satellite Imagery. *arXiv* **2021**, arXiv:2107.12283.
35. Peng, Y.; Fujiyama, M.; Ishida, T. Spatial Evolution of an Oil City: A Case Study of Karamay, Northwest China. *Land* **2022**, *11*, 2011. [CrossRef]
36. Xue, M.; Zhang, X.; Sun, X.; Sun, T.; Yang, Y. Expansion and Evolution of a Typical Resource-Based Mining City in Transition Using the Google Earth Engine: A Case Study of Datong, China. *Remote Sens.* **2021**, *13*, 4045. [CrossRef]